ELSEVIER

Chemical Geology 182 (2002) 697–709

CHEMICAL GEOLOGY
INCLUDING
ISOTOPE GEOSCIENCE

www.elsevier.com/locate/chemgeo

Trace metal fluxes to ferromanganese nodules from the western Baltic Sea as a record for long-term environmental changes

S. Hlawatsch [a], C.D. Garbe-Schönberg [b], F. Lechtenberg [c], A. Manceau [d], N. Tamura [e], D.A. Kulik [f], M. Kersten [g,*]

[a] *GEOMAR, Wischofstr. 1-3, 24148 Kiel, Germany*
[b] *Institute of Geosciences, University of Kiel, Olshausenstr. 40-60, 24118 Kiel, Germany*
[c] *Roentgen-Analytik-Service, Katenkoppel 12, 25524 Itzehoe, Germany*
[d] *Environmental Geochemistry Group, LGIT-IRIGM, CNRS, BP 53, 38041 Grenoble Cedex 9, France*
[e] *Advanced Light Source, Lawrence Berkeley National Laboratory, Berkeley, CA 94720, USA*
[f] *Waste Management Laboratory, Paul Scherrer Institute, CH-5232 Villingen-PSI, Switzerland*
[g] *Geoscience Institute, Gutenberg University, 55099 Mainz, Germany*

Received 20 June 2000; accepted 16 July 2001

Abstract

Trace element profiles in ferromanganese nodules from the western Baltic Sea were analyzed with laser ablation inductively coupled plasma mass spectroscopy (LA-ICP-MS) and synchrotron-based micro-X-ray radiation techniques (fluorescence: μSXRF and diffraction: μXRD) at high spatial resolution in growth direction. Zn showed the only significant enrichment of the trace elements studied (Zn, Cu, Cd, Ni, Co, Mo and Ba), with values in the outermost surface layers of up to sixfold higher than those found in older core parts. The high-resolution Zn profiles provide the necessary temporal resolution for a dating method analogous to dendrochronology. Profiles in various samples collected for two decades were matched, and the overlapping sections were used for an estimation of the accretion rates. Assuming a continuous accretion of these relatively fast-growing nodules (on the average of 20 μm $year^{-1}$ over the last century), the Zn enrichment was assessed to have commenced around 1860/1870 in nodules from the Kiel Bight (BG) and in 1880/1890 in those from Mecklenburg Bight (MB). Apart from the obvious success with Zn, other anthropogenic trace metals like Cu and Cd are not enriched at all, which, together with the distinct early diagenetic Fe/Mn banding, weaken the potential of the nodules for retrospective monitoring.

Keywords: Ferromanganese nodules; Microanalysis; Trace metals; Dating; Baltic Sea

1. Introduction

Accretion of ferromanganese nodules may cover time scales up to millions of years. The implication that they provide a continuously growing substrate with invariable sorption efficiency for trace elements is the basis of a resuming interest for the nodules, focusing on their possible use as a paleoproxy record for long-term environmental changes. Accurate knowledge of the chemical composition and accretion rates is necessary to construct models of the fluxes of these elements into the nodules. Shallow-water Fe/Mn nodules from the Baltic Sea are rela-

* Corresponding author.
E-mail address: michael.kersten@uni-mainz.de (M. Kersten).

0009-2541/02/$ - see front matter
PII: S0009-2541(01)00346-1

tively fast growing which facilitates spatial, and hence, temporal resolution of their geochemical record.

The first evidence for the potential of monitoring anthropogenic impact with these nodules was suggested for samples from the SW Baltic Sea, where Zn was found to be enriched in the outermost layers (Suess and Djafari, 1977). A decade later, similar Zn enrichment was found at another location in the same area (Heuser, 1988). Those observations suggest that metal profiles in ferromanganese nodules could serve even as a tracer of anthropogenic emissions (Glasby et al., 1997; Szefer et al., 1998). The prerequisite for such an approach, however, is high-resolution chemical profiling due to the slow accretion rates of nodules as compared to sediment cores used conventionally for retrospective monitoring (Moenke-Blankenburg et al., 1989; Glasby et al., 1997). Both synchrotron-based micro-X-ray fluorescence (μSXRF) and laser ablation inductively coupled plasma mass spectrometry (LA-ICP-MS) were applied in this study to obtain in situ trace element profiles of the necessary spatial resolution, as a basis for the evaluation of nodule accretion rates and for an assessment of their use for retrospective monitoring of excess anthropogenic metal input into the western Baltic Sea.

2. Material and methods

2.1. Study area

The study area is located in the SW Baltic Sea (Fig. 1). Ferromanganese nodules have been observed in areas with glacial till (boulder clay) exposed through the mud at water depths of 20–25 m. A typical sub-aqueous till rise is represented by the "Blinkerhügel" sampling site in the Mecklenburg Bight (54°10′N, 11°21′E; Fig. 1). The nodules were found mainly as discoidal nodules of a few centime-

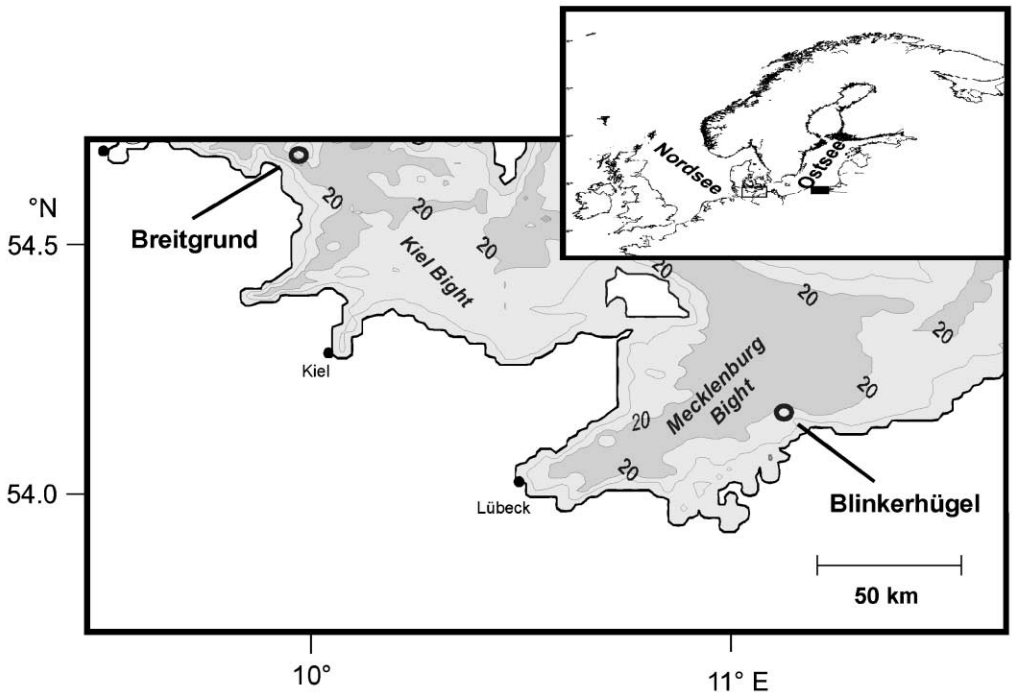

Fig. 1. Location map of the sampling sites "Blinkerhügel" in the Mecklenburg Bight (MB site) and "Breitgrund" in the Kiel Bight (BG site).

ters thick on boulders from lag sediment that accumulated at the boundary between till hills and surrounding mud. The nodules occur just above the centimeter-thick fluffy layer around the boulders like tree mushrooms. The fluffy layer appears to be the major transport belt for the elements that accumulated in the nodules (Hlawatsch et al., in press). For this site denoted as MB, a collection of nodules sampled in 1980 was made available at the Baltic Sea Research Institute in Rostock-Warnemünde. The same site was revisited 14 years later with RV Prof. A. Penck, and "new" samples were taken for the present study. All nodules were carefully collected manually by scuba divers. Four "old" samples from 1980, three "new" samples from 1994, and one additional sample found in 1993 within a dredge from the analogue site "Breitgrund" (BG) in the adjacent Kiel Bight (Fig. 1) were selected and treated by identical sample preparation and analysis. After collection, the samples were soaked in about 500 ml Milli-Q water, rinsed to remove sea salt and oven-dried at 60 °C.

2.2. Trace element analysis

Each sample was broken into half along its longest axis to obtain cross-sections in the direction of highest accretion rates. Subsamples of about 1-mm thickness were scraped off manually by a stainless steel blade for the first screening analysis. Care was taken to trace as much as possible individually visible layers when working inwards along the growth direction from the nodule exterior to the nucleus (Fig. 2). For a quantitative analysis with ICP-OES (Liberty 200, Varian), the subsamples were digested by 2 ml HF + 0.5 ml $HClO_4$ in open PTFE vials until they were dried. The residue was dissolved in concentrated HNO_3 and diluted by nanopure water to the desired volume. The US Geological Survey certified reference material (USGS-CRM) NOD-A-1 was used

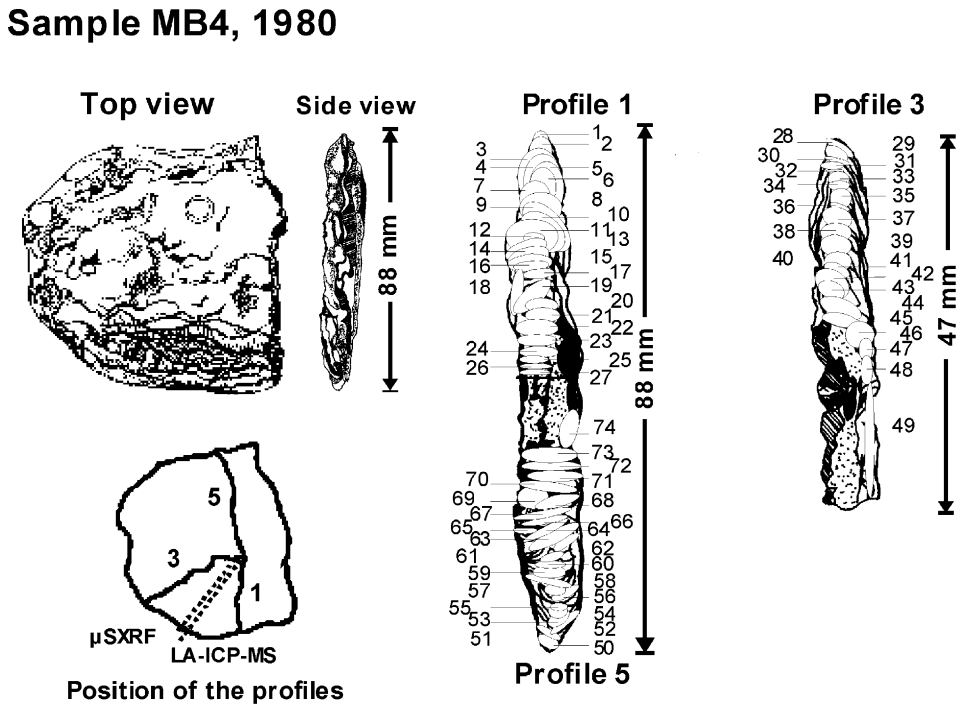

Fig. 2. Morphology and position of analysis profiles cut perpendicular to the flat surface of a representative discoidal ferromanganese nodule (MB4 from the sampling site "Blinkerhügel" in the Mecklenburg Bight) sampled in 1980. The numbers along the depicted profiles 1 and 3 denote individual bands scraped for quantitative ICP-OES analysis. Full characterization of all analyzed samples and compilation of all results are given by Hlawatsch (1999).

for analytical QA/QC. Standard deviation for Mn, Fe, Mg and P was $< 4\%$; for Al, Ca, Zn, Ni, Cr, Co and Mo, $< 6\%$; for K and Li, $< 10\%$; and for Cu, $< 15\%$. Besides USGS-CRM, mill-homogenized nodules from the Mecklenburg Bight have also been used as an internal reference material, with standard deviations of less than $\pm 4\%$ for Mn, Fe, Mg and P; less than $\pm 6\%$ for Al, Ca, Zn, Ni, Cr, Co and Mo; less than $\pm 10\%$ for K and Li; and $\pm 15\%$ for Cu.

For the high-resolution analysis with LA-ICP-MS, subsamples were impregnated with resin, cut into 0.5-cm slices along the growth direction (Fig. 2), polished and mounted on a quartz carrier. For measurements of the elements Li, Al, P, Ca, Mg, Co, Fe, Cr, Cu, Mo, Zn and Pb, a VG Plasma Quad instrument (PQ 1) coupled to a 266-nm UV laser (UV Microprobe, Fisons Instruments) was used as described in detail by Garbe-Schönberg and McMurtry (1994). For best ablation conditions, the laser was focused to a spot size diameter of 50 μm for shots of 2 Hz with 70% energy. The glass CRM NIST 612 and CRM NOD A-1 (as pressed powder pellet) were used for calibration, instrumental drift analysis, and checking for reproducibility of analytical results. The precision of the results was around 15% RSD for most elements.

The μSXRF line scans were performed at beam line L of the Hamburg Synchrotron Radiation Laboratory (DESY/HASYLAB) described in detail by Lechtenberg et al. (1996). The motorized specimen stage was traversed along the growth direction under a stationary beam focused down to a 30-μm spot size. Evaluation of the data was carried out in two steps: (i) spectra background subtraction and characterization of individual element-specific peaks with the software package AXIL (Van Espen et al., 1992), and (ii) quantification of the peaks considering the expected sample composition and spectrometer output with a Monte Carlo simulation code (Vincze et al., 1993). The code is able to calculate the X-ray spectral response of heterogeneous samples irradiated by synchrotron radiation, which requires not only the ability to model all major fluorescence and scattering effects in the full energy range, but also in particular, scattering phenomena of linearly polarized X-rays. Data quality was monitored with the CRMs BHVO-1, GSP-1 and NIST 50, which were analyzed immediately before each sample run. Thus, the estimated standard deviations were $< \pm 5\%$ for Fe, Mn, Zn, Mo and K; $< \pm 10\%$ for Ca, Ni and Cr; and $< \pm 15\%$ for Cu.

The μSRXF element distribution maps and μXRD patterns were recorded on the 7.3.3 microdiffraction beam line at the advanced light source (MacDowell et al., 2001). The fluorescence maps were obtained by scanning a thin section in transmission mode under a monochromatic beam ($E = 10$ keV), with a step size of 10 μm and 1 s of integration time corresponding to a total data collection time of approximately 8 h. The resulting element maps were used to select chemically homogeneous areas for μXRD analysis. The diffractograms were collected using a large-area CCD camera and an exposure time of 10 min. The distance between the analyzed spot on the sample and CCD, together with the 2θ scale, was precisely calibrated using the reflection peaks of quartz grains found in the sample.

3. Results and discussion

3.1. Chemical and mineralogical characterization of the nodule samples

The μSXRF element maps of Fe and Mn (Fig. 3) show typically a cuspate zebra-type band structure consisting of practically pure and alternating Fe- and Mn-rich layers separated by mixed Fe–Mn zones. The thickness of Mn-rich layers varies typically from 200 to 500 μm and that of the Fe-rich layers from about 100 to 200 μm. SEM/EDX analysis revealed a bulk average Mn/Fe ratio of about 3, albeit a high total open pore volume of up to 75% complicates quantitative measurements by microprobe techniques (Glasby et al., 1997). No distinctive diffraction peaks were observed by standard bulk XRD analysis (Hlawatsch, 1999). However, μXRD patterns collected in Mn-rich regions (Fig. 4a) consist of a series of basal reflection peaks at 7.07 (001) and 3.51 Å (002), and *hk*0 peaks at 2.46 (100) and 1.43 Å (110). These peak positions, together with the noteworthy asymmetrical shape of the (100) reflection, are characteristic of turbostratic birnessite (δ-MnO_2; Drits et al., 1997). The absence of *hkl* reflections with index $l \neq 0$ indicates that the phyllomanganate

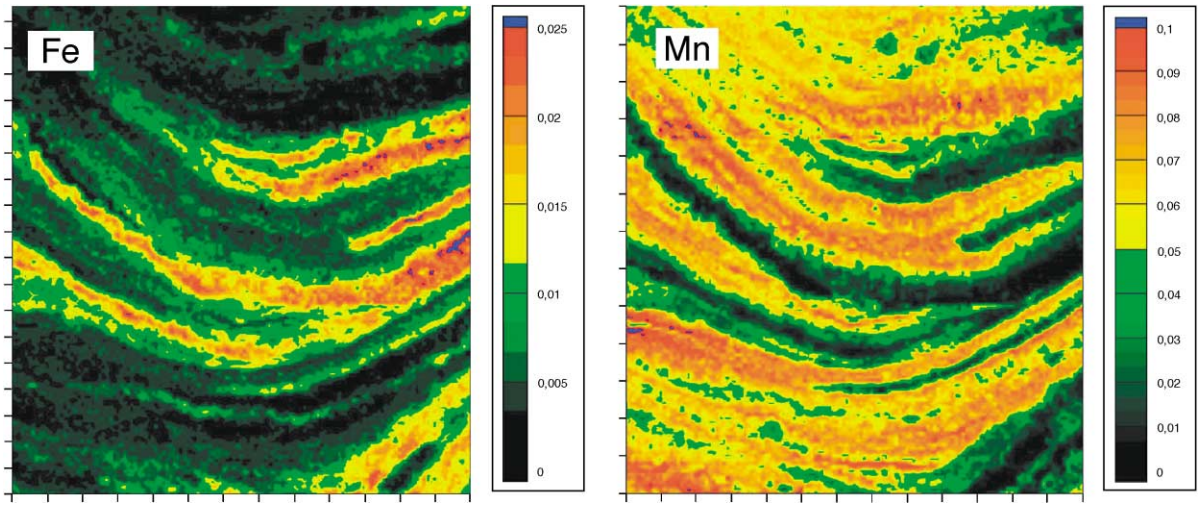

Fig. 3. Synchrotron-based micro-X-ray radiation fluorescence (μSXRF) Fe and Mn maps of a representative area of profile 5 in the nodule sample MB4 from the Mecklenburg Bight (Fig. 2). The scale interval is 100 micrometer and the y-axis represents approximately, from top to bottom. The onion-like structure of growth rims is clearly discernible as few hundreds of micrometer-thick Fe/Mn-rich bandings.

structure is defective with no 3-D periodicity. The μXRD patterns taken in the Fe-rich layers look completely different, revealing only a broad and faint double hump with maxima at about 2.85 and 2.25 Å (Fig. 4b). The centroid of this hump is at about 2.5 Å as in the two-line ferrihydrite (Carlson and Schwertmann, 1981). Minor amounts of detrital quartz grains and silica particles (opal-A?) were also detected by μXRD, which were not at all detectable by bulk XRD analysis.

Similar recent formation of banded iron–manganese nodule structures has been found in other shallow marine (Tazaki, 2000) and even lacustrine (Moore, 1981) environments, which was explained by the Mn/Fe separation due to intermittent oxidizing and reducing conditions, together with some microbiological catalysis. The concretic onion-like growth pattern of alternating Fe- and Mn-rich layers in Baltic Sea ferromanganese nodules has also been attributed to cycling in bottom water redox conditions (Winterhalter and Siivola, 1967; Suess and Djafari, 1977; Ingri and Pontér, 1986; Moenke-Blankenburg et al., 1989; Glasby et al., 1997). Major nodule-forming elements are supplied by pore waters from adjacent anoxic sediments rather than from the water column (Hlawatsch et al., in press). Yearly development of summer anoxia in bottom waters leads to diagenetic remobilization from sediments, lateral transport, diagenetic enrichment and separation of both Mn and Fe in the nodules. Heuser (1988) determined the accretion rates in the order of up to a few tens of $\mu m\ year^{-1}$ of precipitates grown on artificial substrates exposed to this environment. However, these rates varied seasonally, with slower growth from spring to autumn when the water column is stratified. In spring, at the beginning of stratification, the Mn content exceeds that of Fe due to decreasing oxygen concentration in the bottom waters leading to suboxic conditions. In summer, the Fe content may even exceed that of Mn due to occasional anoxia in the bottom water. Partial mobilization of the Mn deposited in the previous autumn may then occur, leaving Fe-enriched layers. With the break-up of the stagnant conditions, the Mn concentrations in the deposits rise again due to the wind-induced aeration of the bottom water. Moore (1981) has already hypothesized that such redox-driven Mn/Fe separation may lead to the well-known banding in shallow-water nodules. The degree of this surficial reduction may depend on the intensity of stagnation. In extreme cases, most of the Mn may be removed from a considerable thickness of nodule, producing a major Fe-rich band. In other times, Mn accretion may continue to be relatively less inter-

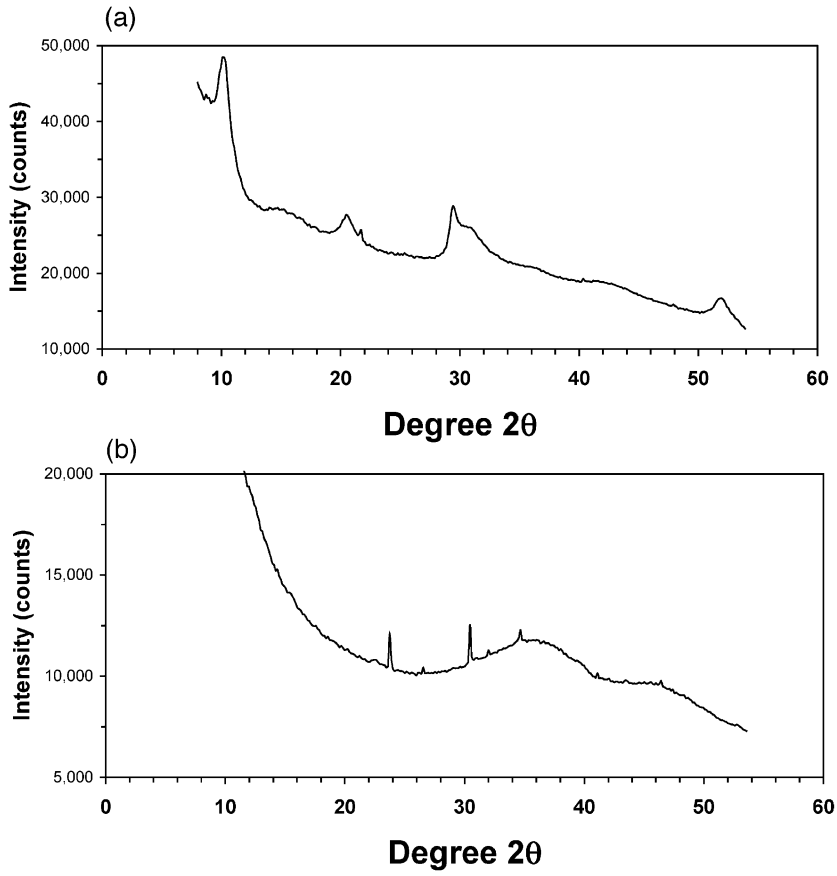

Fig. 4. X-ray microdiffractograms collected in the Mn-rich (a) and Fe-rich (b) regions, with $\lambda = 1.252$ Å (9900 eV) for (a) and 1.758 Å (7050 eV) for (b). Turbostratic birnessite (δ-MnO_2) is the predominating phase identified in (a), while the two-line ferrihydrite is that of (b). Quartz grains (sharp peaks in b) and silica particles ($d \approx 4.6$ Å) were also detected in both regions.

rupted for several years to produce a Mn-rich band. These processes do not necessarily imply that the accretion rates, at least on a short-term scale, are non-steady, but clearly indicate a post-accretional early diagenetic impact on the geochemical record.

3.2. Trace element distribution pattern

The scraping technique analysis already revealed a distinct Zn profile, with concentrations increasing clearly in the outermost sections of the eight studied nodule samples from all sites (Hlawatsch, 1999). Surficial Zn concentrations of more than 1200 μg g^{-1} contrast to a "background" level of about 120 μg g^{-1} in the core of the MB nodules. Other metals, however, do not show any significant enrichment even in the outermost layers. Profiles 1–5 sampled in different growth directions of the same nodule sample (Fig. 2) reflect similar distribution patterns for all elements, just as the profiles of different samples from the same sites. However, the background concentrations in the MB nodules from the Mecklenburg Bight are generally higher than in BG nodules from Kiel Bight. This can be attributed to the slightly lower accretion rate of the MB nodules as discussed below, and to a hot-spot contamination area due to dumping by the "Lübecker Metallhütte" of heavy metal-rich furnace ashes into the Mecklenburg Bight in the 1960s (Leipe et al., 1998).

Comparison and interpretation of both the μSXRF and LA-ICP-MS raw data are difficult due to variations in sample porosity. The laser ablation raw data

readouts were calibrated using the quantitative ICP-OES data. Median values were calculated for the available element concentrations in all three analyzed profiles in crust MB4, and subsequently used for the calculation of response factors for the median values of the raw counts in the analysed laser profile. In this approach, an average porosity is already considered by comparing the ICP-OES with laser data, where only the latter is affected by porosity. Local variation in porosity, however, cannot be corrected because there is no unaffected element that is applicable as an internal standard. Normalization to a constant sum of Fe + Mn should eliminate porosity but actually resulted in even noisier concentration profiles. Moreover, Mn could not be quantified by LA-ICP-MS because of the detector overload on 55 m/z due to the overall high Mn concentrations in the samples. If assuming that Mn concentrations in this profile can be restored from the molybdenum concentrations using $Mn/Mo \approx 1450$ from ICP-OES data for the MB4 profile (24.5 wt.% Mn/169 μg g^{-1} Mo), the average total Mn concentration for the laser profile will be 23.8 wt.% Mn (Table 1). The resulting median value for the Fe/Mn ratio over the complete MB4 profile length of 10 mm is 0.64 which is close to Fe/Mn = 0.65 given by the respective μSXRF and ICP-OES data (Hlawatsch, 1999). Average LA-ICP-MS concentrations for Fe, Mn, Mo, Zn and other relevant trace elements are given in Table 1. Lead turned out to be contaminated in secular spots deriving from the polishing process during sample preparation on a Pb alloy plate, and therefore, will not be considered further on. Comparison of the normalized LA-ICP-MS concentration plots of Fe, P, Mg, Mn, Co, Ni, Cu and Zn (Fig. 5) reveals that only Zn shows a significant steady increase towards the outer zones of the crust, as evidenced already by the quantitative ICP-OES analysis upon their scratching and dissolution.

Table 1
Median values and standard deviation for MB4 profile measurements with LA-ICP-MS ($n = 253$)

Element	Concentration
Fe (wt.%)	14.7 ± 12.8
Mn (wt.%)	23.8 ± 12.8
Fe/Mn	0.64 ± 2.1
Mg (wt.%)	1.41 ± 0.4
Al (wt.%)	0.7 ± 0.3
Ca (wt.%)	1.3 ± 0.4
Li (μg g^{-1})	5 ± 3.6
Cr (μg g^{-1})	54 ± 31.7
Co (μg g^{-1})	66 ± 43.3
Cu (μg g^{-1})	20 ± 4.2
Zn (μg g^{-1})	125 ± 316
Mo (μg g^{-1})	164 ± 188

For the raw μSXRF data, a normalization procedure has been developed, assuming that the bulk of porous solid consists mainly of MnO_2 and FeOOH phases as evidenced above. Both Mn and Fe, and their oxides, have similar gram formula masses (55 and 56; 88 and 89, respectively) and specific densities of ca. 4.2 g cm^{-3}. The quantitative ICP-OES data reveal a strong negative correlation between Mn and Fe concentrations (Hlawatsch, 1999), where the majority of points (in wt.%) plot on a line $C_{Fe} = 40 - 0.9C_{Mn}$. This line would correspond to an average porosity for a compact crust of about 35% in agreement with previous pycnometric estimates by Heuser (1988), and a total $Fe_T + Mn_T$ content of 40–42% (with maximum of 5% of admixture of detrital minerals such as quartz). Hence, the μSXRF data were normalized to a constant of 35% porosity by first deriving a factor f_i (in μg g^{-1}) from Mn and Fe concentrations C_{Fe} and C_{Mn} for each measured data point:

$$f_i = 400{,}000/(C_{Fe} + 0.9C_{Mn}) \quad (1)$$

The concentration of each trace metal C_M at each point is then multiplied by this factor to give its normalized concentration $C_{M,Norm}$:

$$C_{M,Norm} = C_M f_i \quad (2)$$

This procedure strongly reduces the impact of both porosity variations and elevated clastic detritus input, and ultimately renders the μSXRF data comparable to other analytical results. Normalized Fe/Mn ratios are somewhat lower than that from the raw data due to the use of the coefficient 0.9 in Eq. (1). The trend for Zn is generally compatible with that averaged from three parallel LA-ICP-MS shots per profile point, albeit the μSXRF data being still more scattered (Fig. 5C).

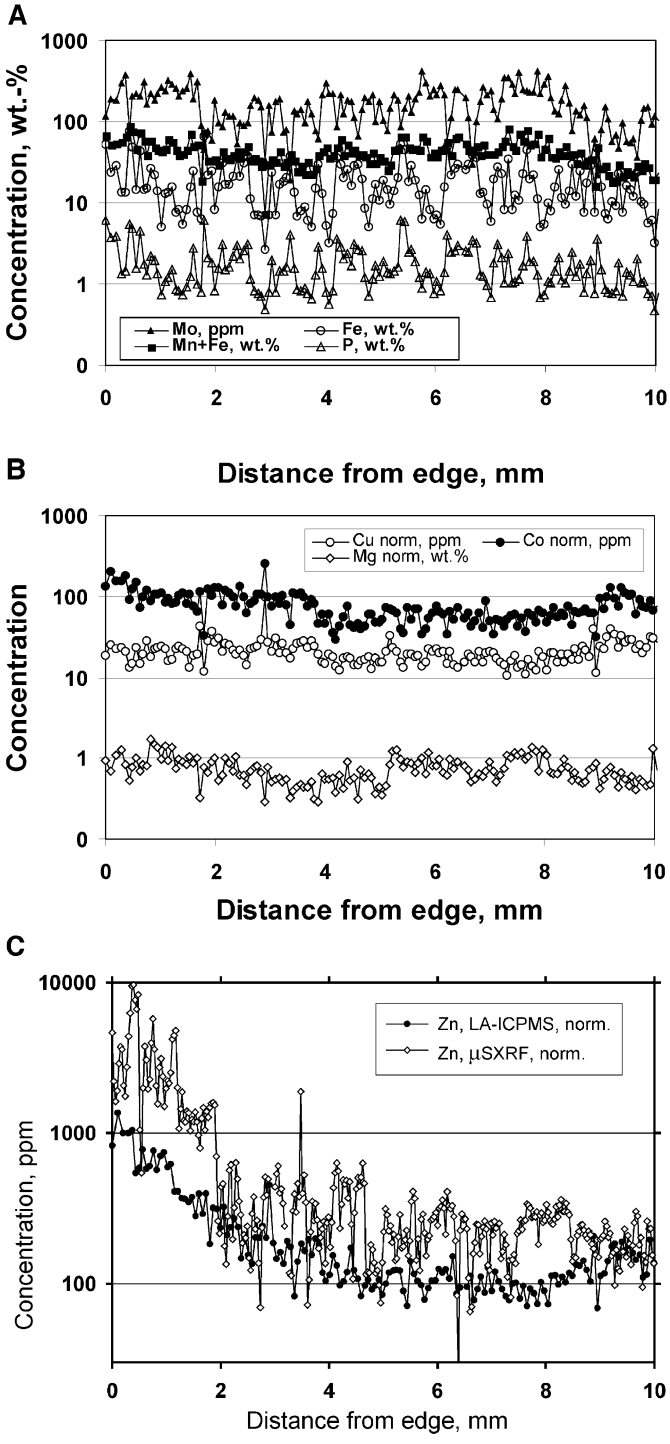
A
Concentration, wt.-%
1000
100
10
1
0
Mo, ppm
Mn+Fe, wt.%
Fe, wt.%
P, wt.%
0
2
4
6
8
10
Distance from edge, mm
B
Concentration
Cu norm, ppm
Co norm, ppm
Mg norm, wt.%
Distance from edge, mm
C
Concentration, ppm
10000
1000
100
Zn, LA-ICPMS, norm.
Zn, µSXRF, norm.
Distance from edge, mm

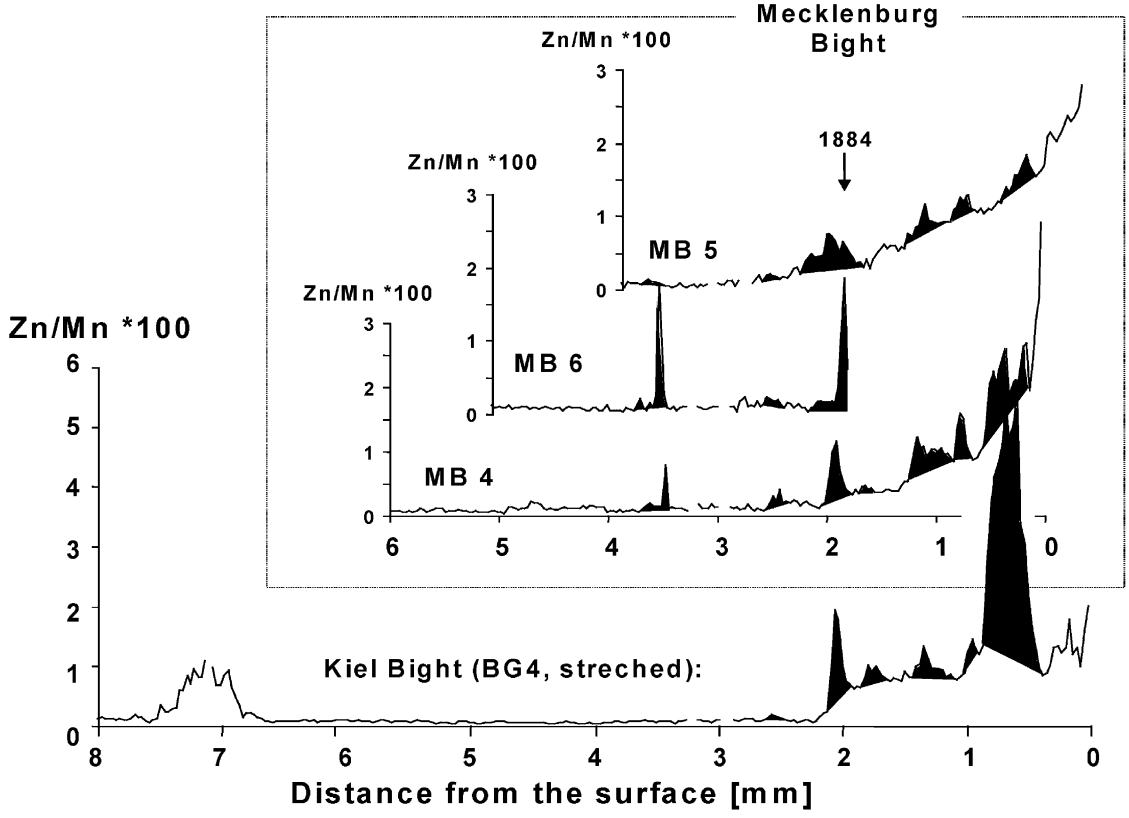

Fig. 6. Distribution pattern of Zn/Mn in the samples MB4, MB5, MB6, and BG4 from μSXRF line scan data. Peaks, which occur in more than one sample, are highlighted. The element ratio was calculated directly from the raw counts. The *x*-axis for BG4 is slightly stretched corresponding to the lower growth rate in the Kiel Bight samples.

3.3. Dating the onset of the anthropogenic Zn enrichment

Results of the high-resolution LA-ICP-MS and μSXRF in situ analyses allow the resolution of individual peaks within the growth layers, providing distinct fingerprint patterns for correlating profiles from different samples. Most prominent is one Zn peak which occurs in the outer rims (Fig. 6). It can be assumed that this pattern indicates the onset of anthropogenic metal enrichment valid for a region larger than the actual sampling site because the peak pattern is coherent for all analyzed samples. This pattern coherence allows for an approach in which Zn distribution patterns in "old" samples are matched to those in "new" samples in a manner analogous to the approach used in dendrochronology (Fig. 7). However, the "new" nodules sampled in 1994 show a thicker section enriched in Zn than the older samples that were collected 14 years earlier. Both patterns must be matched as closely as possible in order to delineate the incremental growth between 1980 and 1994, assuming different but constant accretion rates for both samples during this relatively

Fig. 5. Calibrated LA-ICP-MS data for the MB4 profile: (A) comparison between covarying Fe and P, and inverse-correlated Mo, together with the Mn + Fe pattern; (B) profiles of Co and Cu revealing no significant enrichment towards the crust edge, and that of Mg with no trend over the entire profile, indicating constant support by detrital mineral sources; (C) comparison of both LA-ICP-MS and normalized μSXRF profiles of Zn, with the evident enrichment trend towards the nodule edge.

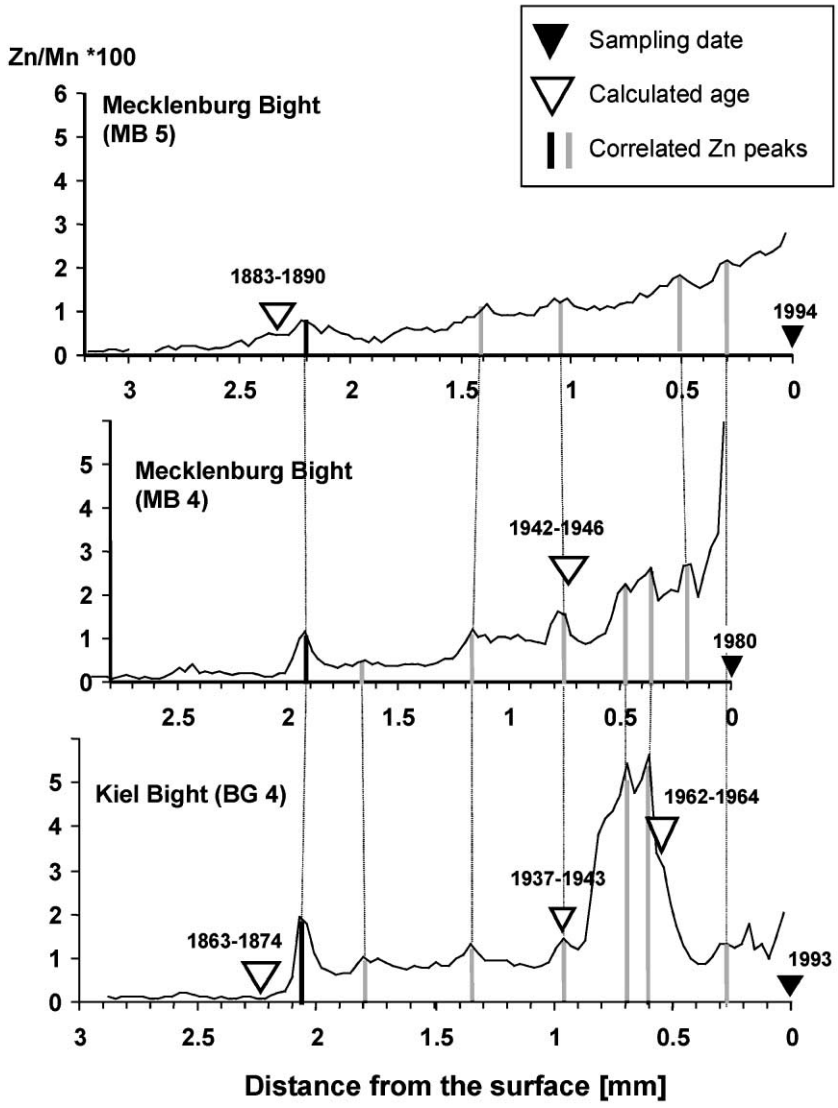

Fig. 7. Evaluation of the nodule accretion rate from the direct comparison of Zn distribution patterns in samples collected at different times. The black lines represent overlying peaks, which were used for pattern correlation according to dendrochronology.

short time span compared to the overall age of the nodules. A set of one "new" and one "old" MB sample was selected for this approach, as well as for comparison, one additional sample from the BG site in Kiel Bight. The pattern match was focused on the peak at the onset of the Zn enrichment. The Zn distribution pattern of the BG sample was slightly stretched to obtain a better fit, which is justified due to the different average accretion rates at the two sites. The zone of Zn enrichment in the sample MB5 from 1994 is 0.30 ± 0.01 mm thicker than that of the sample from the same site collected in 1980. Consequently, the nodule from the MB site grew on average of 0.30 ± 0.01 mm within this time span. The resulting average accretion rate can be estimated to 21 ± 1 μm year^{-1}. Accordingly, the sample BG4 grew on average of 0.23 ± 0.01 mm in 13 years, resulting in an average accretion rate of 18 ± 1 μm

year^{-1}. This is in the order of what is known from lacustrine nodules, but by more than three orders of magnitude faster than what is known for nodules from pelagic sites (Moore et al., 1981a,b).

It is intriguing that the relatively fast average nodule accretion rate of about 20 μm year^{-1} obtained by this simple approach is in the range of that determined by more sophisticated radiometric $^{226}Ra_{ex}$/Ba profiling (7–26 μm: Liebetrau et al., 1999). By interpolation of such accretion rates back to the nucleus, an age of up to more than 4000 years can be estimated for the nodules of the Mecklenburg Bight, which coincides with the post-glacial sea level rise in the Baltic (Limnea stage). Assuming a constant accretion rate at least in the outer 2-mm rim of that nodule, the onset of Zn enrichment at these sites appears to have commenced in the second half of the 19th century, around 1880/1890 at the "Breitgrund" site and in 1870 ± 5 years at the "Blinkerhügel" site. This agrees with the onset of Zn enrichment found in sediments of that area which has also been dated to the end of the 19th century (Erlenkeuser et al., 1974; Leipe et al., 1995). Due to a lack in major river inputs in the SW Baltic, trace metal input is predominantly associated with anthropogenic particles mainly from combustion sources. After World War II, a significant rise in metal and energy production as well as transportation resulted in additional heavy metal emissions. The enhanced Zn emissions during that period are clearly recorded in the nodules, but not that of other metals.

3.4. Metal fluxes to ferromanganese nodules

With the known average accretion rates, metal fluxes into the nodules can now be estimated based on the average concentration of the outermost 2-mm nodule layer using the following approximation:

$$a = \delta c w \quad (3)$$

where a is the metal accumulation rate (μg cm^{-2} year^{-1}); δ is the bulk density with a value of 3.3 g cm^{-3} (Heuser, 1988); c is the metal concentration (in μg g^{-1}); and w is the accretion rate (mm year^{-1}). Thus, the calculated average Mn accretion flux is about 120 μg cm^{-2} year^{-1} for both sites, which is more than 1000-fold higher than for deep-sea nodules (Moore el al., 1981a,b). The resulting Zn scavenging fluxes are 7.2 μg cm^{-2} year^{-1} for the MB site and 4.1 μg cm^{-2} year^{-1} for the BG site. While the P, Ca, Mg, Al and K scavenging fluxes are in the same range as that of Zn, those of the other trace elements are at least one order of magnitude lower and are decreasing in the order Co < Mo < Cu < Ni < Cr < Cu < Li < Cd (Table 2).

Table 2
Accumulation rates of major and trace elements in Fe/Mn nodules

Element	Blinkerhügel 1980 (Mecklenburg Bight)		Breitgrund 1993 (Kiel Bight)	
	Concentration	Flux (μg cm^{-2} a^{-1})	Concentration	Flux (μg cm^{-2} a^{-1})
Mn (%)	17.7	116	18.1	119
Fe (%)	17.2	113	14.5	96
Zn (ppm)	1097	7.2	616	4.1
Cu (ppm)	28	0.19	19.1	0.13
Cd (ppm)	11.5	0.08	b.d.[a]	–
Co (ppm)	170	1.12	60	0.39
Ni (ppm)	93	0.61	67	0.44
Cr (ppm)	67	0.44	70.0	0.46
Mo (ppm)	164	1.08	126	0.83
Li (ppm)	26	0.17	b.d.[a]	–
Mg (%)	1.21	8.0	1.25	8.2
Al (%)	0.94	6.2	1.02	6.7
K (%)	0.87	5.7	0.86	5.7
Ca (%)	1.72	11.3	1.53	10.1
P (%)	1.91	12.6	1.48	9.8

[a] Below detection limit.

4. Conclusion

Trace element accretion profiles in ferromanganese nodules from the SW Baltic Sea were analyzed at a spatial resolution of 30–50 μm with LA-ICP-MS and μSXRF. Both in situ methods allow individual layers of the nodules to be analyzed. The values of both techniques cannot be compared with each other without normalization to constant sample porosity. Among the trace elements studied, only Zn shows a striking profile pattern, with a significant enrichment in the outermost 2-mm surface section. By a fingerprinting approach similar to the one applied in dendrochronology, i.e. direct comparison of Zn distribution patterns in nodule samples collected 14 years apart at the same site, average nodule accretion rates could be estimated at 20 ± 2 μm year^{-1} for both the "Breitgrund" site in the Kiel Bight and the "Blinkerhügel" site in the Mecklenburg Bight. With this relatively fast average accretion rate, the onset of the Zn enrichment could be estimated to commence in 1880/1890 in the Kiel Bight and around 1870 in the Mecklenburg Bight, which coincides with an enhanced rise in anthropogenic metal emissions in the second half of the 19th century.

The relatively rapid accretion is probably one of the main causes for the overall low contents of transition metals in these shallow-water nodules. A major question raised by this study is, however, why no enrichments at all were found for other anthropogenic trace metals like Cu and Cd. One plausible explanation was advocated by Hlawatsch et al. (in press), who found strong neutral to negative charged aqueous complexes by voltammetric measurements for both Cu and Cd in the supporting suboxic fluffy layer, and suggested that these metals are therefore less available for scavenging. On the other hand, it can be assumed that the record of the nodules consists of actually emitted elements on top of a probably dominating amount provided by redox-driven secondary geochemical remobilization processes. Such an early diagenetic impact may, in general, has decreased Mn contents in the nodules, but at the same time, enhanced contrasts in the composition of adjacent bands, leading to strong depletion of certain layers in Mn and simultaneous formation of Fe/Mn banding. Such a post-accretional transformation of the substrate geochemistry may also lead to a repartitioning of some of the trace metals as discussed in a subsequent paper, but clearly acts towards the averaging and smoothing of the primary input signal which weakens the value of the nodule profiling for retrospective anthropogenic trace metal monitoring as already suggested earlier by Ingri and Pontér (1986).

Acknowledgements

The authors wish to thank Capt. Albrecht and his crew of the RV Prof. A. Penck, and the scuba diver groups of IOW, as well as A. Kordian for the excellent support at the sampling site; the beam line scientists of HASYLAB (G. Falkenberg) and ALS (A. A. MacDowell, R. S. Celestre and H. A. Padmore) for the continuing development and support with the microfocusing beam lines; D. Benesch, R. Rosenberg, J. Schulz, G. Böttcher, A. Ulrich, R. Bahlo and T. Arpe for sample preparation and chemical analysis; A. Dahmke, J. Harff, R. Heath, F. Manheim, T. Leipe, D. Rickert, P. Sachs, P. Stoffers, and E. Suess for support and discussions; and last but not least, the editor, Eric Oelkers and three anonymous reviewers for valuable comments. This study was supported by a German Science Foundation grant (HA 1834/3), by the LBNL Laboratory Director's Research and Development Fund (ALS microdiffractometer beam line measurements) and by the US Department of Energy Office of Basic Energy Sciences Contract No. DOE-AC03-765F00098.

References

Carlson, L., Schwertmann, U., 1981. Natural ferrihydrite in surface deposits from Finland and their association with silica. Geochim. Cosmochim. Acta 45, 421–429.

Drits, V.A., Silvester, E., Gorshkov, A.V., Manceau, A., 1997. Structure of synthetic monoclinic Na-rich birnessite and hexagonal birnessite: I. Results from X-ray diffraction and selected-area electron diffraction. Am. Mineral. 82, 946–961.

Erlenkeuser, H., Suess, E., Wilkomm, H., 1974. Industrialization effects of heavy metal and carbon isotope concentrations in recent Baltic Sea sediments. Geochim. Cosmochim. Acta 38, 823–842.

Garbe-Schönberg, C.-D., McMurtry, G.M., 1994. In situ micro-

analysis of platinum and rare earth elements in ferromanganese crusts by Laser Ablation-ICP-MS (LA-ICP-MS). Fresenius' J. Anal. Chem. 350, 264–271.

Glasby, G.P., Emelyanov, E.M., Zhamoida, V.A., Baturin, G.N., Leipe, T., Bahlo, R., Bonacker, P., 1997. Environments of formation of ferromanganese concretions in the Baltic Sea: a critical review. In: Nicholson, K., Hein, J.R., Bühn, B., Dasgupta, S. (Eds.), Manganese Mineralization: Geochemistry and Mineralogy of Terrestrial and Marine Deposits. Geol. Soc. Spec. Publ. 119, 213–237.

Heuser, H., 1988. Beobachtungen und Untersuchungen zur Genese von Flachwasser-Manganknollen in der Kieler Bucht (westliche Ostsee). Reports Geol. Paläont Inst. Univ. Kiel, vol. 26. ICES, Germany.

Hlawatsch, S., 1999. Mn–Fe-Akkumulate als Indikator für Schad- und Nährstoff flüsse in der westlichen Ostsee. GEOMAR Reports, vol. 85. ICES, Germany.

Hlawatsch, S., Neumann, T., van den Berg, C.M.G., Kersten, M., Harff, J., Suess, E., 2001. Fast-growing shallow-water Fe/Mn nodules: origin and modes of incorporation of trace elements. Mar. Geol. (in press).

Ingri, J., Pontér, C., 1986. Scavenging properties of ferromanganese nodules in the Gulf of Bothnia. ICES Reports, Copenhagen, vol. 186, pp. 234–243.

Lechtenberg, F., Garbe, S., Bauch, J., Dingwell, D.B., Freitag, J., Haller, M., Hansteen, T.H., Ippach, P., Knöchel, A., Radtke, M., Romano, C., Sachs, P.M., Schmincke, H.U., Ullrich, H.J., 1996. The X-ray fluorescence measurement place at beam line L of Hasylab. J. Trace Microprobe Tech. 14, 561–587.

Leipe, T., Neumann, T., Emeis, K.-C., 1995. Schwermetallverteilung in holozänen Ostseesedimenten-Untersuchungen im Einflußbereich der Oder. Geowissenschaften 13, 470–478.

Leipe, T., Tauber, F., Brügmann, L., Irion, G., Hennings, U., 1998. Schwermetallverteilung in Oberflächensedimenten der westlichen Ostsee Arkonabecken, Mecklenburger/Lübecker Bucht und Kieler Bucht. Meyniana 50, 137–154.

Liebetrau, V., Frei, R., Eisenhauer, A., Hansen, B.T., 1999. Mn/Fe concretions record the last 4300 years of Pb isotope variations in Baltic seawater. EUG XI J. Conf. Abstr., vol. 6. Cambridge Publ., Oxford, p. 222.

MacDowell, A.A., Celestre, R.S., Tamura, N., Spolenak, R., Valek, B.C., Brown, W.L., Bravman, J.C., Padmore, H.A., Batterman, B.W., Patel, J.R., 2001. Submicron X-ray diffraction. Proc. 7th Intern. Conf. Synchrotron Rad. Instrum. Nucl. Inst. Phys. Res. A 467, 936–943.

Moenke-Blankenburg, L., Jahn, K., Brügmann, L., 1989. Laser-micro-analytical studies on distribution patterns of manganese, iron and barium in Mn–Fe accumulates of the western Baltic Sea. Chem. Erde 49, 39–46.

Moore, W.S., 1981. Iron–manganese banding in Oneida Lake ferromanganese nodules. Nature 292, 233–235.

Moore, W.S., Dean, W.E., Krishnaswami, S., Borole, D.V., 1981a. Growth rates of manganese nodules in Oneida Lake, New York. Earth Planet. Sci. Lett. 46, 191–200.

Moore, W.S., Teh-Lung, K., MacDougal, J.D., Burns, V.M., Burns, R., Dymond, J., Lyle, M.W., Piper, D.Z., 1981b. Fluxes of metals to a manganese nodule: radiochemical, chemical, structural and mineralogical studies. Earth Planet. Sci. Lett. 52, 151–171.

Suess, E., Djafari, D., 1977. Trace element distribution in Baltic Sea ferromanganese concretions: interferences on accretion rates. Earth Planet. Sci. Lett. 35, 49–54.

Szefer, B., Glasby, G.P., Kunzendorf, H., Görlich, E.A., Latka, K., Ikuta, K., Ali, A.A., 1998. The distribution of rare earth and other elements and the mineralogy of the iron oxyhydroxide phase in marine ferromanganese concretions from within Slupsk Furrow in the southern Baltic. Appl. Geochem. 13, 305–312.

Tazaki, K., 2000. Formation of banded iron–manganese structures by natural microbial communities. Clays Clay Miner. 48, 511–520.

Van Espen, P., Janssens, K., Swenters, I., 1992. AXIL X-ray analysis software. Manual and Computer Program. University of Antwerpen, Belgium.

Vincze, L., Janssens, K., Adams, F., 1993. A general Monte Carlo simulation of energy dispersive X-ray fluorescence spectrometers. Spectrochim. Acta 48B (4), 553–573.

Winterhalter, B.T., Siivola, B., 1967. An electron microprobe study of the distribution of iron, manganese and phosphorus in concretions from the Gulf of Bothnia, northern Baltic Sea. C. R. Soc. Geol. Finl. 39, 161–172.